THE JOURNAL OF PHYSICAL CHEMISTRY A

Article

Conical for Stepwise, Glancing for Concerted: The Role of the Excited-State Topology in the Three-Body Dissociation of *sym*-Triazine

Vadim A. Mozhayskiy, John D. Savee, Jennifer E. Mann, Robert E. Continetti, and Anna I. Krylov

J. Phys. Chem. A, **2008**, 112 (48), 12345-12354 • Publication Date (Web): 30 October 2008

Conical for Stepwise, Glancing for Concerted: The Role of the Excited-State Topology in the Three-Body Dissociation of *sym*-Triazine

Vadim A. Mozhayskiy,[†] John D. Savee,[‡] Jennifer E. Mann,[‡] Robert E. Continetti,[‡] and Anna I. Krylov*,[†]

Department of Chemistry, University of Southern California, Los Angeles, California 90089-0482, and Department of Chemistry and Biochemistry, University of California at San Diego, 9500 Gilman Drive, La Jolla, California 92093-0340

Received: July 18, 2008; Revised Manuscript Received: September 3, 2008

The highly debated three-body dissociation of *sym*-triazine to three HCN products has been investigated by translational spectroscopy and high-level ab initio calculations. Dissociation was induced by charge exchange between the *sym*-triazine radical cation and cesium. Calculated state energies and electronic couplings suggest that *sym*-triazine is produced in the 3s Rydberg and $\pi^* \leftarrow$ n manifolds. Analysis of the topology of these manifolds along with momentum correlation in the dissociation products suggest that the 3s Rydberg manifold characterized by a conical intersection of two potential energy surfaces leads to stepwise dissociation, while the $\pi^* \leftarrow$ n manifold consisting of a four-fold glancing intersection leads to a symmetric concerted reaction.

1. Introduction

Dissociation of energetic molecules is one of the most fundamental processes in chemistry.[1] In atmospheric, planetary, and biochemical reactions, dissociation is often induced by photoexcitation, whereas in high-temperature environments (e.g., combustion), there is sufficient thermal energy to break bonds.

Proliferation of novel experimental and theoretical techniques has enabled physical chemists to gain increasingly more detailed mechanistic insights into dissociation processes. Experimentally, it has become possible to observe chemical transformations in a more direct fashion, for example, to investigate dynamics of a well-characterized initial state rather than ensemble averages, and even monitor bond breaking in real time by means of femtosecond spectroscopy. The development of experimental techniques has been paralleled by advances in theory, which progressed from qualitative interpretations to rigorous quantitative predictions in electronic structure and dynamics.

Yet, our understanding of the dissociation of polyatomic molecules is rather incomplete, even for processes as fundamental as a three-body breakup.[2,3] Since the first report of a three-body dissociation of azomethane in 1929,[4] only about 30 systems capable of three-body photodissociation were characterized.[2] Among these, there are only six molecules that produce three molecular fragments, azomethane, *s*-tetrazine, triazine, acetone, DMSO, and glyoxal. More examples of three-body breakup have been observed in dissociative recombination and photodetachment.[5] In dissociative recombination, where more energy is available, three-body dissociation becomes a dominant channel for many systems. Unfortunately, the dynamical information available in those studies is quite limited because those experiments are typically performed in ion storage rings at very high beam energies.

For almost every one of the above examples of three-body breakup, there is a history of controversy of whether the dissociation proceeds in a stepwise or a concerted fashion. The mechanistic controversy stems from the challenges of characterizing the dissociation of a polyatomic system at the molecular level. Several of the reactions are believed to be true "triple whammy" events proceeding through symmetric transition states and involving simultaneous (i.e., within one rotational period) breaking of two bonds. These reactions become even more fascinating when one realizes that the reverse reaction is a termolecular association reaction and is generally improbable on account of collision statistics. Yet, termolecular reactions are important, the most prominent example being ozone formation in which a three-body reactive collision is an essential part of the mechanism:[6] $O_2 + O + M \rightarrow O_3 + M$.

sym-Triazine (Tz), the largest among the few molecules studied to date capable of photoinduced three-body breakup, is the only one that produces three polyatomic products. Moreover, due to its high symmetry, it produces three identical fragments

$$C_3N_3H_3^* \rightarrow 3HCN \qquad (1)$$

This unique feature of Tz facilitates unambiguous mechanistic interpretation of the dynamics; indeed, the symmetric kinetic energy distribution among the three fragments can only be observed in the concerted three-body process.

The concerted mechanism proposed in earlier studies of Tz dissociation has been a subject of considerable debate.[7−12] In the photofragment translational spectroscopy (PTS) experiments,[7,8] dissociation was initiated by 248 and 193 nm photoexcitation most likely into the $\pi^* \leftarrow$ n and $\pi^* \leftarrow \pi$ manifolds, respectively, but dissociation to three HCN occurs ultimately through decay to the ground state, as dictated by symmetry correlation arguments and energy balance.[13] The original PTS study by Ondrey and Bersohn assumed that the HCN photoproducts were produced in a concerted fashion and, therefore, received an equal kinetic energy release (KER);[7] however, the later work by Gejo et al. presented evidence in favor of stepwise dissociation.[8] Ab initio calculations of transition states along with classical trajectory studies have found that the barrier to a symmetric concerted reaction lies lowest in energy, but the studies have suggested that at higher excitation energies, the stepwise mechanism could become more prevalent.[9−12]

* To whom correspondence should be addressed.
[†] University of Southern California.
[‡] University of California at San Diego.

10.1021/jp806369s CCC: $40.75
Published on Web 10/30/2008

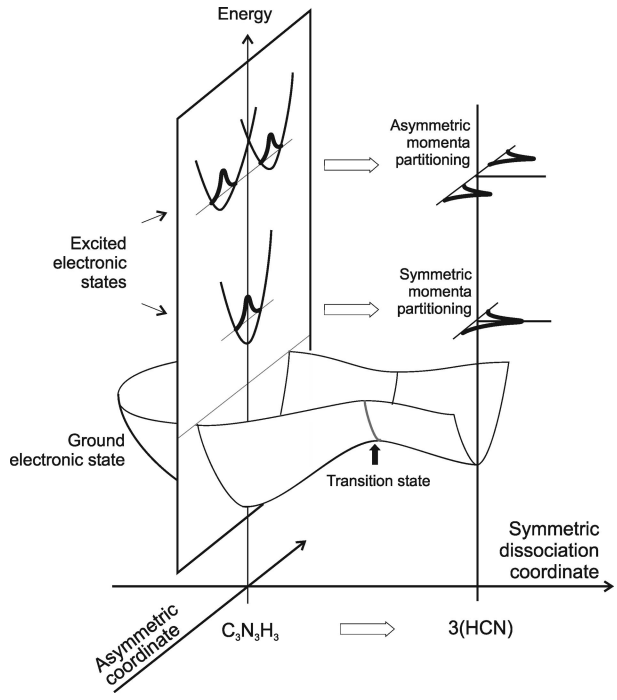

Figure 1. Two-dimensional representation of the ground- and excited-state PESs, demonstrating mapping of the initial wave function into the product distribution, that is, reflection principle. The two coordinates are the reaction coordinate for the three-body dissociation and a symmetry-lowering displacement, for example, Jahn−Teller deformation. The reflection principle, which assumes ballistic dissociation on the lowest PES, predicts symmetric energy partitioning for the process initiated on the symmetric PES and asymmetric energy partitioning for a distorted one.

We report the first direct observation of the symmetric three-body breakup of Tz by using coincidence detection of neutral products coupled with translational spectroscopy, which allows a full kinematic description of the process. Coincidence experiments, which are capable of unambiguously distinguishing between symmetric and asymmetric dissociation, are no longer limited to ionic products.[14] Continetti and co-workers extended this technique to neutral species, and it has been applied to H_3.[15,16]

Dissociation is initiated by charge exchange (CE) between Tz^+ and cesium, a technique for producing electronically excited neutral molecules.[17−19] We have observed products with both symmetric (i.e., equal between the three fragments) and C_{2v} (further referred to as "asymmetric") momentum partitioning corresponding to two fast and one slow or two slow and one fast fragments. The former case suggests a concerted three-body breakup, while the latter is consistent with stepwise decomposition. While the underlying dissociation dynamics may be very complex and involve multiple electronic states, the reflection principle[20] suggests that the two processes proceed through at least two different electronic states with symmetric (D_{3h}) and asymmetric equilibrium geometries, as illustrated in Figure 1.

A key feature noted for CE experiments is the potential to excite multiple initial electronic states.[17] If CE occurs in a resonance regime, Tz is expected to be excited above its ground state by 6.12 eV,[21] that is, the difference between ionization energies of Tz and cesium (10.01 and 3.89 eV, respectively). However, the amount of energy deposited in neutrals created by CE of keV cation beams and alkali electron donors can also occur off resonance, with transition probabilities depending on the energy defect, coupling strength, and relative velocity between the cation and electron donor.[17,18,22] We found that the relative ratio of symmetric versus asymmetric momentum partitioning depends on the beam velocity, which suggests that different excited states are populated and consequently decay via different mechanisms. To elucidate the nature of the initially excited state and to determine how it influences the mechanism of the three-body breakup, we performed ab initio calculations of excited-state potential energy surfaces (PESs) and couplings. The calculations and analysis of several Jahn−Teller (JT) manifold topologies allowed us to identify the most likely initially populated states as the A_1 3s Rydberg and the A_2 π^* ← n valence states.

It should be noted that the influence of initially excited electronic states on the outcome of a reaction in the ground state is not new to chemistry. For example, mechanisms of photochemical reactions are often explained by structures of relevant conical intersections, as was done by Mebel and co-workers in their study of Tz photodissociation.[9] Recently, Suits and co-workers[23] argued that the selection between different channels of propanal cation dissociation occurs because the molecule finds itself in different configurations in the ground state given different starting points (i.e., cis or gauche conformations) in the excited state. The motif suggested by the present work is different. As evidenced by geometry optimizations of electronically excited states[24] and the PES scans presented below, the distortions of electronically excited Tz are relatively small owing to a relatively rigid π-system. Thus, the molecule is unlikely to sample vastly different conformations, and the momentum partitioning is influenced by whether or not there is a vibrational excitation in asymmetric modes.

A brief report on this work, which presents the first full coincidence investigation of a three-body dissociation producing three neutral polyatomic fragments, has been recently published.[25] The goal of this paper is to present a more in-depth discussion on the electronic aspects of the three-body dissociation of Tz. We will briefly review the experimental methods and results and focus on the electronic structure and CE probability calculations.

2. Experimental Methods and Computational Details

2.1. Experimental Methods. The fast-beam translational spectrometer capable of detecting multiple neutral fragments in coincidence is a modified version of a previously described apparatus.[26] Tz^+ was produced using an electrical discharge in a 1 kHz pulsed supersonic expansion (25 psig of backing pressure) of a mixture of room-temperature Tz (97%, Alfa Aesar) vapor seeded in 250 psig of He. Cations were then skimmed, electrostatically accelerated to 12 or 16 keV, and rereferenced to ground using a high-voltage switch. The cation of interest ($m/z = 81$) was mass-selected by time-of-flight and electrostatically guided through a 1 mm^3 interaction region containing Cs vapor (approximately 10^{-5} Torr). Any unreacted cations were deflected out of the beam path and monitored with an ion detector. Neutrals formed in the interaction region were allowed to propagate 110 cm forward to a time- and position-sensitive microchannel plate based delay-line anode.[27] The neutral particle detector was capable of coincidence detection of the time and position of arrival for up to eight particles in a single event, given a favorable recoil geometry. Given the beam energy, parent cation mass, and fragment masses, a full three-dimensional kinematic description of the dissociation process was obtained, including the center-of-mass-frame KER and product momentum partitioning.

Empirical product KER distributions were constructed for the three-body dissociation of Tz upon CE of the Tz^+ with Cs at

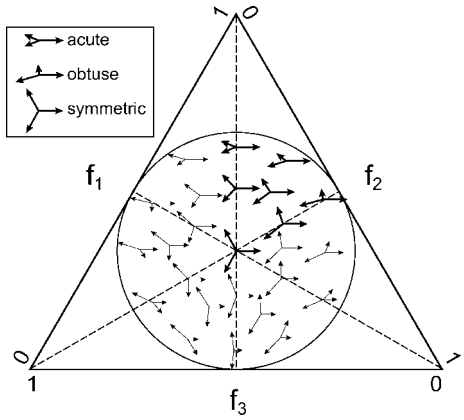

Figure 2. The Dalitz plot represented as a map of the momentum partitioned to three equal-mass fragments. Each axis of the Dalitz plot corresponds to the squared fraction of the momentum imparted to one of the three fragments. The center point of the plot corresponds to the equal momentum partitioning. Dashed lines represent regions of C_{2v} symmetry within the plot, which correspond to one fast and two slow (acute feature) or to one slow and two fast (obtuse feature) fragments.

both 12 and 16 keV cation beam energies. Due to the finite size of the neutral particle detector, certain events were not detected. Monte Carlo simulations of the detector's geometric efficiency were used to correct the empirical distributions to produce true probability distributions, denoted as P(KER).[16,28] A similar procedure employing Monte Carlo simulations was also used to correct the Dalitz plots presented below.

2.1.1. The Dalitz Plot. Momentum and energy partitioning in three-body dissociation can be most clearly examined using a correlated method of displaying the data such as a Dalitz plot,[29] which is an equilateral triangle with each axis corresponding to the fractional square (f_i) of the momentum $\vec{p}_i$ imparted to a single neutral fragment:

$$f_i = \frac{|\vec{p}_i|^2}{\sum_i |\vec{p}_i|^2} \tag{2}$$

In short, a single point on the three-axis plot within the inscribed circular region of momentum conservation represents a specific arrangement of three momentum vectors pointing from the center-of-mass (c.m.) of the system to the c.m. of the recoiling fragments, as shown in Figure 2. Thus, the Dalitz plot is a histogram of events, and the intensity on the plot corresponds to the number of recorded events with a particular momentum distribution. Since Tz dissociates to three indistinguishable equal-mass HCN fragments, the plot exhibits a six-fold degeneracy and three-fold symmetry. Note that the momentum vectors represented in the Dalitz plot are constructed from final c.m. frame trajectories. For concerted dissociation, the Dalitz plot can be used to identify an instantaneous impulsive force driving the fragments apart. However, the final c.m. frame trajectories in a stepwise process are the result of several intermediate events and not readily apparent in the Dalitz plot alone.

Monte Carlo simulations were used to interpret characteristic features observed in Dalitz distributions in the present experiment. While the symmetric Dalitz feature discussed below represents a concerted process, the mechanism giving rise to the C_{2v} feature is not as apparent. To determine how a stepwise mechanism would manifest itself in the Dalitz plot, we conducted ad hoc Monte Carlo simulations, which will be described in detail elsewhere.[30] The simulations demonstrated that the acute feature can indeed be interpreted as the result of a stepwise reaction.

2.2. Theoretical Methods and Computational Details. Electronically excited states of Tz were computed using the equation-of-motion coupled-cluster method with single and double substitutions (EOM-EE-CCSD)[31−34] employing the 6-311++G** basis set. The cation states were described by the EOM-CC method for ionized states, EOM-IP-CCSD.[35,36] Electronic states of the combined $(Cs-Tz)^+$ system were characterized by EOM-EE-CCSD using a closed-shell reference state corresponding to the lowest electronic state of the Cs^+-Tz system. The Hay−Wadt effective core potential basis set with an additional polarization function with an exponent of 0.19 for a Cs atom was suggested by Glendenning et al.,[37] along with the 6-311+G* basis set for C, H, and N atoms.

The advantage of EOM-CC methods is that they allow a balanced description of multiple electronic states of different nature, for example, Rydberg and valence, degenerate JT states, interacting charge-transfer (e.g., Cs^+-Tz^* and $Cs-Tz^+$) states, and so forth. Moreover, the EOM-CC wave functions for the electronically excited and ionized states of Tz employ the same closed-shell reference, that is, the ground electronic state of Tz. This feature facilitated calculation of electronic coupling elements governing the CE process.

The EOM-EE wave functions of the combined $(Cs-Tz)^+$ system were used to evaluate the diabatic electronic couplings (h_{ab}) between the $Cs-Tz^+$ and Cs^+-Tz^* states (i.e., quantities that control CE) by the generalized Mulliken−Hush (GMH) method.[38,39] The GMH method developed by Cave and Newton to compute the diabatic−adiabatic transformation matrix and the coupling elements is based on the assumption that there is no dipole moment coupling between the diabatic states, and thus, the dipole moment matrix is diagonal in this representation. This corresponds to the two states with the largest charge separation, that is, charge localized on the reactants and products. The so-defined transformation matrix can hence be applied to the Hamiltonian matrix in the adiabatic representation, yielding the coupling as the off-diagonal element. This leads to the following expression:

$$h_{ab} = \frac{\mu_{12}\Delta E_{12}}{\left[(\Delta\mu_{12})^2 + 4(\mu_{12})^2\right]^{1/2}} \tag{3}$$

where the letter and number subscripts refer to diabatic and adiabatic quantities, respectively, μ_{12} is the transition dipole moment, $\Delta\mu_{12}$ is the difference between the permanent dipole moments, and ΔE_{12} is the energy gap between the states. These couplings were used to evaluate probabilities of populating different electronic states in the CE process using the Demkov model,[40] as described below.

PES scans for the $(Cs-Tz)^+$ electronic states were computed in two steps. First, the total energies for the $(Cs-Tz)^+$ system were calculated for the Tz part at the neutral ground-state geometry and Cs atom on the C_3 symmetry axis of Tz^+ by varying the $Cs-Tz^+$ distance. Asymptotic values of these energies are identical to the excitation energies of Tz and are given in Table 1. Then, the energies were shifted to account for the JT relaxation of the Tz^+ core such that each excited state of the $(Cs-Tz)^+$ complex asymptotically approached vertical excitation energies of Tz at the cation geometry at infinite separation (15 Å). This was done by subtracting differences in excited energies at the neutral and cation geometries from Table 1. In addition, the energies of $Cs-Tz^+$ excited states (i.e., neutral Cs atom, initial state of Tz in the experiment) were shifted to match the asymptotic value of 6.12

TABLE 1: Vertical EOM-EE-CCSD/6-311++G Excitation Energies (eV) for Tz at the Neutral (D_{3h}) and the Cation (C_{2v}) Ground States Geometries[a]**

	singlets				triplets			
	D_{3h}		C_{2v}		D_{3h}		C_{2v}	
$\pi^* \leftarrow$ n	$^1A_1''$	4.99	$^1A_2$	4.53	$^3A_2''$	4.53	$^3B_1$	4.34
	$^1A_2''$	5.04	$^1B_1$	4.78	$^3E''$	4.71	$^3A_2$	4.32
	$^1E''$	5.06	$^1B_1$	5.30			$^3B_1$	4.87
			$^1A_2$	5.53	$^3A_1''$	4.99	$^3A_2$	5.37
$\pi^* \leftarrow \pi$	$^1A_2'$	6.01	$^1B_2$	6.49	$^3A_1'$	4.80	$^3A_1$	5.23
	$^1A_1'$	7.54	$^1A_1$	8.14	$^3E'$	5.82	$^3B_2$	6.24
	$^1E'$	8.43	$^1A_1$	>8.6			$^3A_1$	6.32
			$^1B_2$	>8.6	$^3A_2'$	6.83	$^3B_2$	7.40
$R_s \leftarrow$ n	$^1E'$	7.41	$^1A_1$	7.03	$^3E'$	7.34	$^3A_1$	6.97
			$^1B_2$	7.71			$^3B_2$	7.64
$R_p \leftarrow$ n	$^1A_2'$	8.24	$^1B_2$	7.90	$^3A_1'$	8.08	$^3A_1$	7.81
	$^1E'$	8.25	$^1A_1$	7.84	$^3A_2'$	8.23	$^3B_2$	7.87
			$^1B_2$	8.60	$^3E'$	8.26	$^3B_2$	8.57
	$^1A_1'$	8.29	$^1A_1$	8.61			$^3A_1$	>8.6
$\pi^* \leftarrow n_2$	$^1E''$	8.18	$^1A_2$	8.31	$^3E''$	7.58	$^3B_2$	7.68
			$^1B_1$	8.53			$^3A_1$	7.75

[a] All energies are relative to the ground-state energy of neutral Tz at the respective geometries. To recalculate energies relative to three ground-state HCN molecules, 1.86 eV should be subtracted.

eV at infinite separation (the difference between the experimental IE of cesium and Tz, 3.89 and 10.01 eV, respectively).

The PES scans for the ground and electronically excited states of Tz along the symmetric three-body dissociation coordinate were computed by EOM-EE-CCSD/6-311++G** using the geometries obtained by Pai et al.[12] for the dissociation reaction coordinate on the MP2/6-31G** ground-state PES.

All calculations were performed using the Q-Chem electronic structure program.[41]

3. Results and Discussion

Reaction mechanisms are ultimately defined by the shape of the underlying PES, and the interpretation of both experimental observations and theoretical predictions requires the knowledge of structures and energies of the PES stationary points, for example, barriers and local minima along the reaction coordinates. The mechanisms of processes that span more than one electronic state also depend on the couplings and crossings between different PESs. Below, we will discuss important features of the relevant PESs, as well as calculations of electronic couplings determining CE probabilities.

A necessary condition for concerted dissociation is the existence of an energetically accessible appropriate transition state, and many theoretical studies of the interplay between concerted and stepwise mechanisms have focused on locating and comparing different transition states.[42−47] Tz has an accessible symmetric transition state for the three-body dissociation;[12] however, a complete picture of the mechanism requires information about dynamics, which depends on how the process was initiated. This aspect of the dynamics—the effect of initial conditions on the reaction outcome—can be understood within the reflection principle framework.[20] In photodissociation, the reflection principle assumes a ballistic process (i.e., no vibrational equilibration) on the excited-state surface, which therefore acts as a mirror reflecting the initial wave packet onto the final states of the products. In the present experiment, the roles of excited- and ground-state surfaces are reversed; Tz is prepared in an electronically excited state, and the dissociation occurs ultimately in the ground electronic state. For the three-body breakup on the PES with the symmetric transition state, the reflection principle predicts a symmetric KER for the initially symmetric wave packet and an asymmetric KER for the initial conditions described by the asymmetric wave packet, as explained in Figure 1. The shape of the initial wave packet is determined by the shape of the corresponding excited-state surface on which Tz is produced by CE. Since all of the electronically excited states of Tz in the relevant energy region are derived by transitions between doubly degenerate orbitals, some of them will themselves be degenerate and therefore subject to asymmetric JT distortions. However, some of the states have symmetric PES by virtue of double degeneracy of both the initial and the target molecular orbitals (MOs) and can, therefore, result in a symmetric wave packet.[48,49]

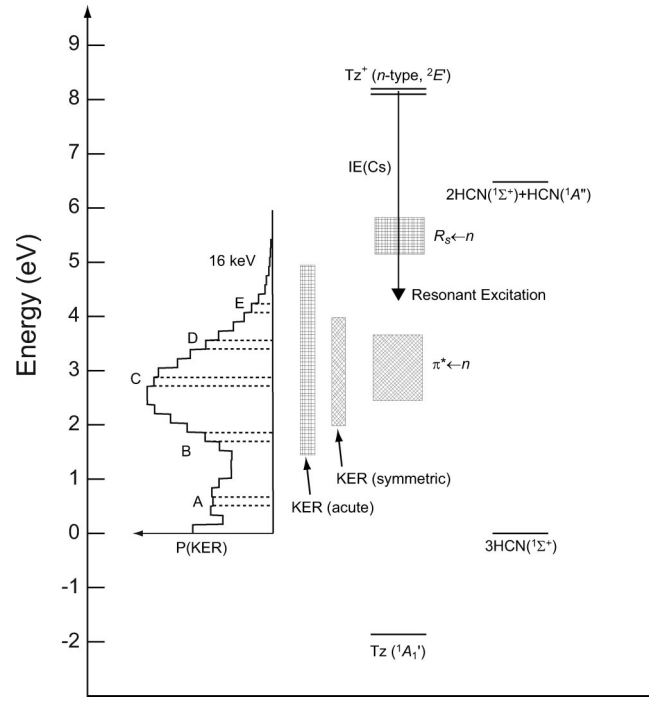

Figure 3. Energy diagram for the three-body dissociation of Tz. The *P*(KER) distribution obtained with a 16 keV cation beam is shown on the left. Labeled KER intervals correspond to the following energies: A(0.51−0.68 eV), B(1.69−1.86 eV), C(2.70−2.87 eV), D(3.38−3.54 eV), E(4.05−4.22 eV). The hatched boxes labeled "KER (acute)" and "KER (symmetric)" mark the region over which the mechanism was observed. The hatched boxes labeled "3s Rydberg" and "$\pi^* \leftarrow$ n" denote the regions between the lowest and the highest lying states (triplets included) in each manifold, as computed at the cation equilibrium geometry (C_{2v}). Zero energy corresponds to the ground-state energy of three HCNs.

3.1. Kinetic Energy Release and Dalitz Plots. Figure 3 shows the *P*(KER) distribution for dissociation following CE of a 16 keV beam of Tz^+ with Cs, accompanied by the relevant dissociation limits, calculated electronic state minima, and energy thresholds. *P*(KER) distributions obtained at 12 and 16 keV are similar and extend from 0 to 5 eV with a major feature peaked at 2.6 eV and a minor feature at 0.5 eV relative to the three ground-state HCN molecules. On the basis of the Tz enthalpy of formation[50] (ΔH_f = 225.87 kJ/mol), CE in the resonance regime should produce Tz* 4.26 eV above the 3 HCN($X^1\Sigma^+$) limit. However, the maximum observed KER extends well beyond this limit, suggesting a degree of nonresonant excitation in the CE process.

We found that the three-body momentum distribution depends strongly on the KER. To illustrate this dependence, *P*(KER) distributions were divided into 32 KER bins, and Dalitz representations[29] (see section 2.1.1) were used to visualize the

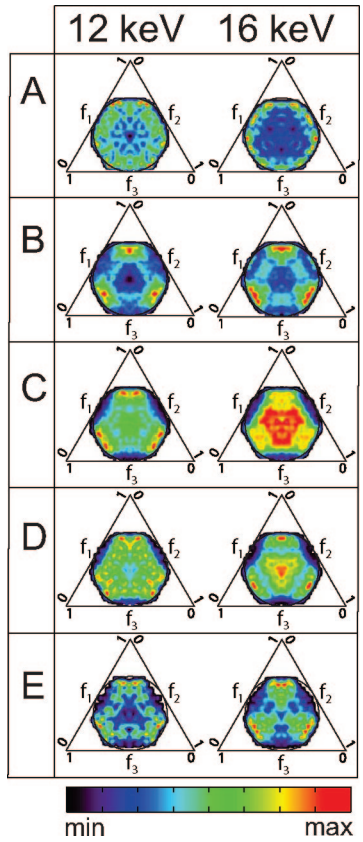

Figure 4. Dalitz representations of the momentum correlation in the three-body breakup of Tz obtained over KER intervals denoted in Figure 3. A symmetric partitioning of momentum yields intensity in the center of the Dalitz plots, whereas the intensity near the apexes (i.e., acute features) corresponds to one fast and two slow fragments.

momentum partitioning for the events contained within each KER bin. Several Dalitz representations constructed from the 12 and 16 keV Tz data are shown in Figure 4 and correspond to the labeled KER ranges in Figure 3. A two-fold symmetric acute feature (two slow and one fast HCN fragment) dominates the Dalitz representations between intervals B and E at both beam energies. A weaker feature corresponding to a three-fold symmetric partitioning of momentum is also present, and the Dalitz distributions in Figure 4 have been slightly cropped near the intense acute apexes in order to highlight it. While more apparent in the 16 keV Dalitz plots, the symmetric feature is present (along with the acute feature) for intervals C and D at both beam energies. This symmetric feature also exhibits slight asymmetries extending toward the two-fold symmetric obtuse region of the Dalitz plot.

Dalitz distributions were constructed for intervals spanning the entire *P*(KER) distribution and reveal the ranges over which the acute and symmetric Dalitz features were observed as 1.5−5 and 2−4 eV, respectively (denoted in Figure 3). These two seemingly independent features and the dependence of their relative ratio on the beam energy suggest that dissociation proceeds by two different mechanisms, the origins of which were an impetus for the ab initio investigation into the electronic structure of Tz.

Without performing nonadiabatic dynamics simulations in full dimensionality (as, for example, in refs 51 and 52) and on multiple PESs, one can gain mechanistic insight by using simple Franck−Condon considerations and the reflection principle,[20] as sketched in Figure 1. In our energy range, the three-body dissociation necessarily proceeds in the ground state, and the transition state for this process is symmetric.[9−12] Assuming ballistic dissociation on the ground-state PES (and neglecting possible involvement of other electronic states in the nonadiabatic relaxation from the initially populated electronic state to the ground state), the reflection principle states that dumping a symmetric nuclear wave packet on the ground-state PES results in the symmetric dissociation, whereas a nonsymmetric process corresponds to a nonsymmetric nuclear wave function. Asymmetric wave packets give rise to vibrational excitation of asymmetric modes, which ultimately leads to asymmetric momentum partitioning. Thus, the symmetric and asymmetric channels can be explained by two different initial electronic states of neutral Tz, one with three-fold symmetry (D_{3h}) and one with lower symmetry (e.g., C_{2v}), assuming that the vibrational wave function equilibrates in the excited state prior to electronic relaxation. To elucidate the nature of the initially populated states, we performed electronic structure calculations of the excitation energies, coupling elements, and PES scans as described below. In light of the dense electronic spectrum of Tz, only by considering several characteristics of the excited states, their excitation energies, nonadiabatic couplings, and the topologies of the corresponding JT manifolds, were we able to identify the most likely initially populated states as the A_1 3s Rydberg and the A_2 $\pi^* \leftarrow$ n valence states.

TABLE 2: The GMH Couplings (h_{ab}) for CE between Cs and the Triazine Cation at 5 and 8 Å Cs−Tz$^+$ Separations[a]

	5 Å Cs−Tz$^+$ Separation			
	$\Delta\mu_{12}$, au	ΔE_{12}, eV	$\mu_{1,2}$, au	h_{ab}, eV
$\pi^* \leftarrow$ n	5.40	−0.15	0.080	0.002
$\pi^* \leftarrow \pi$	5.44	0.80	0.000	0.000
$R_s \leftarrow$ n	−1.00	1.85	2.640	0.909
$R_p \leftarrow$ n	−0.36	2.00	1.563	0.993
	8 Å Cs−Tz$^+$ Separation			
	$\Delta\mu_{12}$, au	ΔE_{12}, eV	$\mu_{1,2}$, au	h_{ab}, eV
$\pi^* \leftarrow$ n	11.04	−0.35	0.040	0.001
$\pi^* \leftarrow \pi$	11.06	0.55	0.000	0.000
$R_s \leftarrow$ n	3.40	0.95	4.360	0.443
$R_p \leftarrow$ n	−0.37	1.80	0.473	0.838

[a] The couplings are computed by eq 2 using the dipole moment difference ($\Delta\mu_{12}$), energy separation (ΔE_{12}), and transition dipole moments ($\mu_{1,2}$).

3.2. Electronic States of *sym*-Triazine and Electronic Couplings between the Cs−Tz$^+$ and Cs$^+$−Tz States. The electronic spectrum of Tz consists of dense manifolds of valence $\pi^* \leftarrow \pi$ and $\pi^* \leftarrow$ n states,[21,53−56] as well as Rydberg states derived from the transitions from nitrogen lone pairs (n) and π orbitals. While in the ground electronic state, Tz is of D_{3h} symmetry, and many of the excited states, as well as the cation,[57,58] are distorted by virtue of the JT theorem.

Our calculations[24] identified more than 20 states of neutral Tz below 9 eV. Examination of the energy diagram in Figure 3 and the computed excitation energies summarized in Table 1 reveals that several singlet and triplet states are accessible energetically, that is, all of the $\pi^* \leftarrow$ n and $\pi^* \leftarrow \pi$ states, as well as the lowest Rydberg $R_s \leftarrow$ n state.

Electronic couplings between the Cs−Tz$^+$ and Cs$^+$−Tz* states (i.e., initial and final states in a CE event) computed by the GMH approach[38,39] (see section 2.2) are presented in Table 2. In agreement with qualitative considerations,[17] the calculations show that the couplings between the Cs−Tz$^+$ and different Cs$^+$−Tz* states are at least 400 times larger for the Rydberg states than those for the valence states. Furthermore, the $\pi^* \leftarrow$

π values are nearly zero due to the two-electron character of the corresponding electronic transition (the ground state of Tz^+ has a hole in a lone pair orbital).[58] The same arguments apply to the corresponding triplet states, which are accessible in CE experiments. Thus, considerable electronic coupling matrix elements for the 3s Rydberg and $\pi^* \leftarrow$ n manifolds suggest these states as the most likely initially populated electronic states. However, the coupling for the Rydberg state is two orders of magnitude larger than that of the $\pi^* \leftarrow$ n state. As noted by Peterson and co-workers,[17] CE transitions between loosely bound orbitals (hence, characterized by large couplings) would yield large cross sections, whereas CE between tightly bound orbitals occurs mostly in close collisions and is characterized by small cross sections. More quantitative analysis of how couplings of these magnitudes will manifest themselves in branching ratios of the two channels can be obtained using the Demkov model,[40] as described in the next section.

3.3. Evaluation of CE Probabilities Using the Demkov Model. To discriminate between the different states, we employ the simple two-state Demkov model to evaluate transition probabilities for the CE process.[40] The transition probability derived from this model depends upon the potential energy difference (i.e., the off-resonant energy defect), the potential parameter in the coupling matrix element, and the relative velocity between the cation and atomic electron donor:

$$\omega = \mathrm{sech}^2\left(\frac{\pi}{2\sqrt{2mI}} \cdot \frac{\Delta E}{V}\right)\sin^2\left(\int_{-\infty}^{+\infty} h_{ab}\mathrm{d}t\right) \qquad (4)$$

where ΔE is the energy defect (energy difference between the $Cs-Tz^+$ and Cs^+-Tz states), h_{ab} is a matrix coupling element between the two states, V is the relative velocity, and t, m, and I denote time, mass, and the smaller of the ionization energies of electron donor or acceptor, respectively. This semiclassical model is derived by assuming that the coupling h_{ab} increases exponentially at short distances and approaches zero as the fragments scatter apart. The maximum value of the coupling should be on the order of the energy defect ΔE, and the latter is assumed to be constant in the exchange region.

The first term in eq 4, $\mathrm{sech}^2(...)$, is the CE transition probability amplitude, which increases with the relative velocity V and asymptotically approaches unity. At a 12 keV energy, this term can be rewritten as $\mathrm{sech}^2(\alpha^{\mathrm{eff}}_{12\mathrm{keV}}\Delta E)$, where all constants and the scattering velocity dependence are included in the effective cross section parameter $\alpha^{\mathrm{eff}}_{12\mathrm{keV}}$. At any other beam energies, E_b, the cross section term equals $\mathrm{sech}^2[\alpha^{\mathrm{eff}}_{12\mathrm{keV}}\Delta E(12/E_b)^{1/2}]$, where $\alpha^{\mathrm{eff}}_{12\mathrm{keV}}$ is the effective cross section parameter at 12 keV. Figure 5 shows the CE cross sections as a function of beam energy for the two states with energy defects of 0.2 and 1.0 eV using two different values of $\alpha^{\mathrm{eff}}_{12\mathrm{keV}}$ (5 and 1 eV^{-1}). The top panel showing the cross section for $\alpha^{\mathrm{eff}}_{12\mathrm{keV}} = 5\ \mathrm{eV}^{-1}$ corresponds to the α value before the saturation, which seems to be the case in the present experiment. As one can see from Figure 5, the cross section increases (and saturates) faster for smaller energy defects.

The second term in eq 4, $\sin^2(...)$, describes the population oscillation between the two states, $Cs-Tz^+$ and Cs^+-Tz. The frequency of the oscillation is proportional to the electronic coupling matrix element integrated over the interaction time. For the Rydberg Cs^+-Tz states, the coupling h_{ab} is about 1 eV (0.037 hartree; see Table 2). Assuming an interaction region of $\sim$15 au, the time of interaction between Tz^+ and Cs is about 5×10^{-15} s (200 au) at a 12 keV beam velocity. With the exponential increase of the coupling from 0 to 0.037 hartree and the decrease back to 0 over 200 au of time, the value of

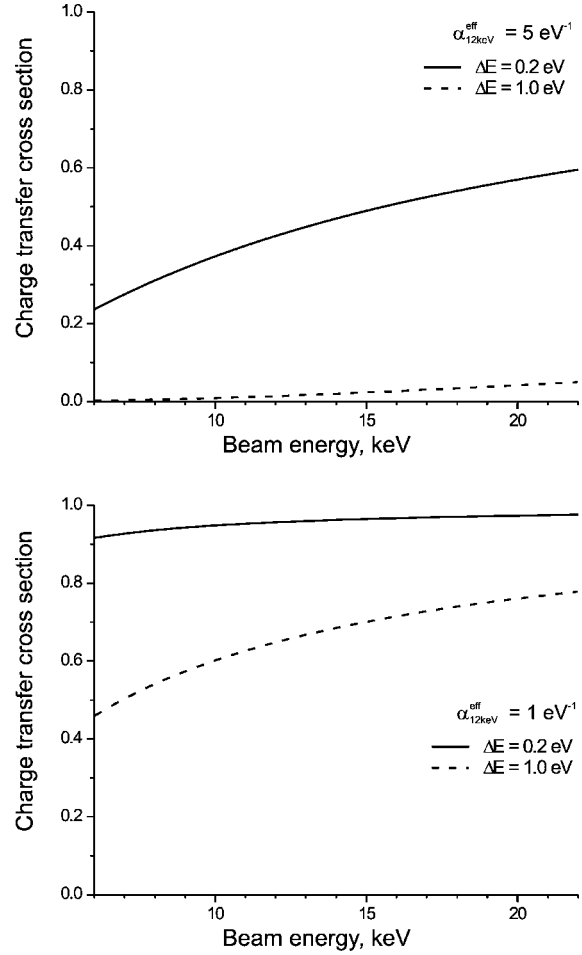

Figure 5. The CE cross sections as a function of beam energy for the two states with energy defects of 0.2 (solid line) and 1.0 eV (dashed line) at a 12 keV beam energy. The upper and lower panels show that the results for the effective cross section parameter $\alpha^{\mathrm{eff}}_{12\mathrm{keV}}$ equal 5 and 1 eV^{-1}, respectively.

the effective coupling $h^{12\mathrm{keV}}_{\mathrm{eff}} = \int_{-\infty}^{+\infty} h_{ab}\mathrm{d}t$ is estimated as 5 au. For a beam energy E_b other than 12 keV, the effective coupling is given by

$$h_{\mathrm{eff}}(E_b, \mathrm{keV}) = \sqrt{\frac{12}{E_b}}h^{12\mathrm{keV}}_{\mathrm{eff}} \qquad (5)$$

since the interaction time is inversely proportional to the square root of the relative velocity. The top panel in Figure 6 shows strong oscillations in the value of the $\sin^2(...)$ term with the phase depending strongly on the exact value of the coupling. In the experiment, there are variations in the effective coupling due to the variety of the impact parameters and orientations of Tz, and the $\sin^2(...)$ term values are averaged[59] with an effective value of $\sim$0.5 for the Rydberg states (see Figure 6). The coupling for the valence states from the $\pi^* \leftarrow$ n manifold is two orders of magnitude smaller, which results in an almost constant value of the $\sin^2(...)$ term with respect to the Tz^+ beam velocity. The value of this oscillating term is $\sim$400 times smaller for the valence $\pi^* \leftarrow$ n state that than for the Rydberg state, as shown in the bottom panel in Figure 6.

Thus, for a given interaction time determined by the neutral−ion relative velocity, the model predicts a larger probability for populating states with (i) a smaller energy defect (i.e., in resonance) and (ii) a larger coupling. The velocity dependence of the branching ratios between different channels

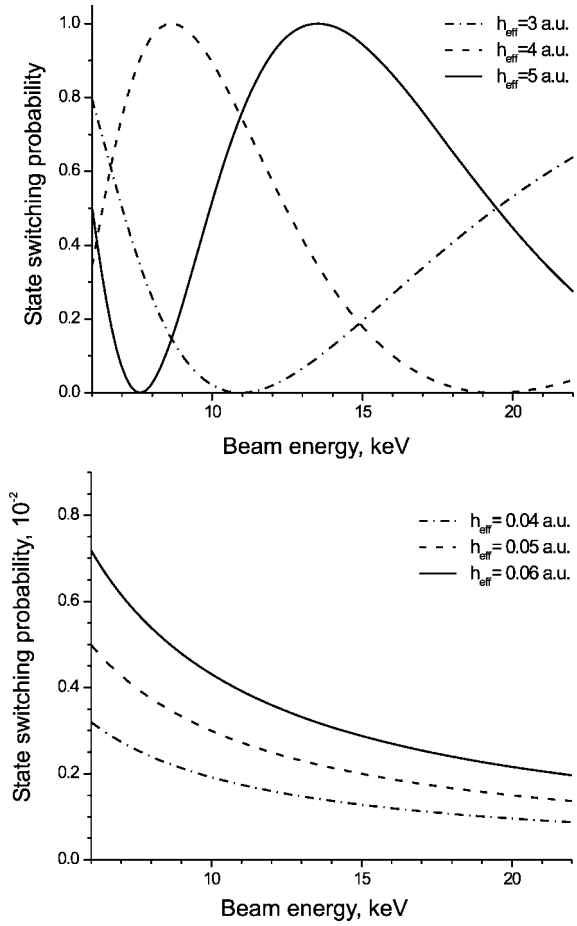

Figure 6. The state switching probability term, $\sin^2(...)$ in eq 4, as a function of the Tz^+ beam energy for selected values of effective couplings (eq 5) on the order of magnitude corresponding to the R ← n (top panel) and π^* ← n (bottom panel) states at 12 keV.

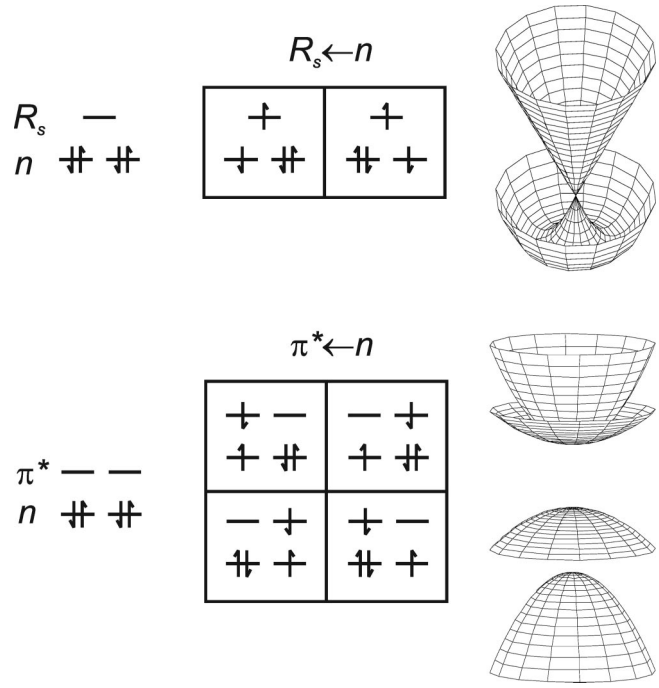

Figure 7. Topology of regular (upper panel) and four-fold (lower panel) Jahn−Teller intersections. The former case corresponds to the states derived from the transitions between doubly degenerate and nondegenerate MOs. Four-state intersections occur for the states originating from the transitions between the two sets of doubly degenerate MOs. Symmetry analysis predicts that two out of four states will be exactly degenerate at D_{3h}. While the topology and degeneracy pattern might differ, the PES of the upper state always has a (nearly) symmetric minimum.

is nonlinear and is determined chiefly by the energy defect through the cross section (eq 5). The probability of populating the state with a smaller energy defect increases more rapidly than that of the state with a larger defect as the relative ion−atom velocity increases. Thus, the observed velocity-dependent change in the relative intensity of the two features from Figure 3 suggests that two different initial electronic states of the neutral give rise to the observed dissociation channels. The dominant character of the asymmetric channel suggests stronger couplings for the respective initial state, whereas the increased intensity for the symmetric dissociation at 16 keV argues in favor of the smaller off-resonant energy defect of the corresponding state.

Energy defects of the Rydberg and π^* ← n states (0.75 and 0.66 eV asymptotically) reveal that neither state is in exact resonance, although the valence state is 0.1 eV closer. However, as will be demonstrated in section 3.5, at short Cs−Tz^+ distances, the valence state becomes nearly degenerate with the Cs−Tz^+ state, whereas the energy defect of the Rydberg state increases.

Thus, the Demkov model predicts a much higher probability of populating the Rydberg state, even though it is further off-resonance compared to the π^* ← n state. The respective equilibrium geometries of these states can be considered as starting points on the neutral ground-state surface by virtue of the reflection principle (see Figure 1).

3.4. Analysis of the Excited State's Topology. It is possible to determine which of the excited states have symmetric equilibrium structures, and which are distorted, by simply analyzing symmetries and the electronic configurations of the corresponding wave functions, as in recent studies of N_3^+.[48,49] All of the states discussed above are derived from transitions involving degenerate MOs and can, therefore, be potentially subject to JT distortions. States derived from the transitions between degenerate and nondegenerate MOs (e ⊗ a → E) form a familiar "Mexican hat"-shaped PES shown in Figure 7. The pair of R_s ← n Rydberg states in Tz is of this type. A qualitatively different type of intersection occurs for the states derived from excitations between two degenerate MO pairs producing two exactly degenerate and two nearly degenerate states, that is, e ⊗ e → E + A + B. It can be shown that all four states are scrambled around the intersection, and the linear terms for the degenerate states are very small.[48,49] Consequently, the intersection appears to be glancing rather than conical, as shown in Figure 7. Although the minimum of the upper degenerate PES is not exactly at D_{3h}, a small magnitude distortion (e.g., 0.001 Å and 10^{-4} eV in cyclic N_3^+) suggests a negligible effect on the corresponding nuclear wave functions, which, therefore, could be treated as derived from the symmetric PES. As will be discussed in an upcoming paper,[24] the minimum of the top π^* ← n state of Tz is numerically almost exactly at D_{3h}.

3.5. The PES Scans. Figure 8 shows the PES scans along the symmetric three-body dissociation coordinate for the ground and the lowest electronically excited states of Tz. Note that none of the excited states correlate with the dissociation limit of the three ground-state HCN. Moreover, the excited-state curves are rather parallel to the ground-state one and feature a barrier along the three-body dissociation coordinate. Thus, Figure 8 suggests that there are no obvious conical intersections between the

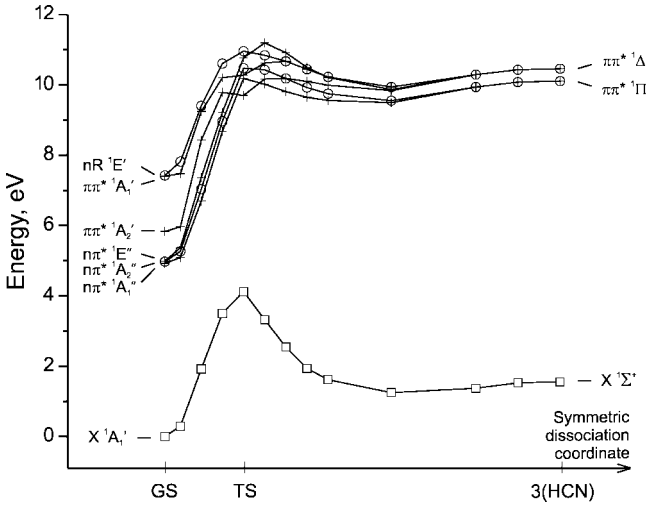

Figure 8. Potential energy curves for the ground and excited states of Tz along the symmetric three-body dissociation coordinate.

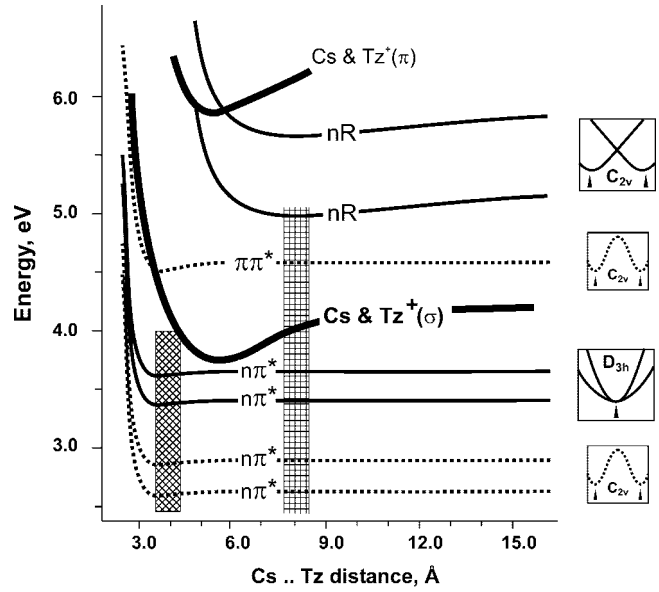

Figure 9. Potential energy curves for the relevant singlet electronic states of the $(Cs-Tz)^+$ system in a T-shaped configuration. Bold and light curves correspond to $Cs-Tz^+$ and Cs^+-Tz states, respectively, whereas solid and dashed lines distinguish between the valence and Rydberg excited states. The geometry of the triazine fragment is that of the cation. The pictograms on the right show the PES topology for each state along the JT coordinate. As in Figure 3, the shaded boxes denote the KER regions for which symmetric and asymmetric dissociations were observed. Energies are relative to the ground-state energy of three HCN.

ground and the excited states in the proximity of the dissociation coordinate. A nondissociative character of the excited state's PES suggests that nonadiabatic relaxation is likely to occur in the FC region. One can therefore expect slow radiationless relaxation to the ground state, which will allow electronically excited Tz* to vibrationally equilibrate prior to the transition. Of course, only nonadiabatic dynamics calculations in full dimensionality can reveal where (and how fast) Tz* reaches the ground-state PES; however, the presently available data support the above mechanism for symmetric dissociation. The S_1-S_0 conical intersection reported by Dyakov et al.[9] is at the opened ring geometry and thus would lead to the asymmetric momenta partitioning among the fragments.

Figure 9 shows a scan of the calculated PESs for Cs approaching Tz^+ in a direction perpendicular to the molecular plane. Bold and light curves correspond to the $Cs-Tz^+$ and Cs^+-Tz states, respectively. At infinite separation, the state ordering is exactly as that in neutral Tz at the cation geometry. The pictograms on the right show the topology of each PES around D_{3h}. Note that the diffuse $R_s \leftarrow n$ states become perturbed by approaching Cs at 7 Å, while the PESs of the valence states remain flat up to about 3.5 Å. This numerically demonstrates the qualitative statement made by Peterson and co-workers[17] regarding the necessity of close collisions for electron capture into valence states.

Analysis of the topology shows that among the states in the energy range corresponding to the symmetric dissociation, the only states with a symmetric equilibrium structure are the upper $\pi^* \leftarrow n$ states, as denoted by the pictograms in Figure 9. Thus, we conclude that these states are responsible for the symmetric channel. The asymmetric dissociation may occur via all other states accessible energetically; however, the most likely candidate is the lowest Rydberg $R_s \leftarrow n$ state for which the GMH coupling is two orders of magnitude larger than that for the valence states. Thus, we conclude that acute and symmetric dissociations occur following initial excitation into the 3s Rydberg and $\pi^* \leftarrow n$ manifolds, respectively. This assignment is supported by qualitative agreement between the observed intensity of these channels and the GMH matrix coupling elements.

The energetic locations of the 3s Rydberg and $\pi^* \leftarrow n$ manifolds in the cation Franck−Condon region correlate well with the KER range over which each Dalitz feature was observed. The maximum observed KER of 5 eV associated with the acute feature is close to the vertical energy for the Rydberg states (i.e, 5.17 and 5.11 eV above the three HCN limit for the singlet and triplet, respectively). Monte Carlo simulations support the acute Dalitz feature being the result of a stepwise dissociation.[30] The maximum observed KER of 4 eV for symmetric dissociation lies 0.33 eV higher in energy than the vertical energy of the highest $\pi^* \leftarrow n$ state ($^1A_2$), which is located at 3.67 eV above the three HCN limit and has a D_{3h} equilibrium structure. The small separation between the singlet and triplet states does not allow us to discriminate between these manifolds. However, due to the three-fold degeneracy of the triplets, one might expect triplets to be populated more frequently. On the other hand, the rate of electronic relaxation to the ground-state singlet PES is likely to be much slower for the triplets.

Finally, we would like to comment on the obtuse lobes of the "symmetric" Dalitz feature, which shows slight asymmetries associated with the symmetric mechanism. Possible explanations for these features are (i) that the electronic transition to the ground-state PES occurs too fast, that is, while the molecule still has vibrational excitation in an asymmetric mode (expected to be populated because of the JT distorted geometry of the cation), as suggested by Dyakov et al.;[9] (ii) that crossing to an intermediate lower-symmetry electronic state occurs prior to dissociation; and (iii) that contributions from the initial population of nearby distorted $\pi^* \leftarrow n$ states. Interestingly, it was observed that excitation into the $\pi^* \leftarrow n$ manifold results in a partially asymmetric "symmetric" dissociation, which agrees with recent theoretical predictions aimed at resolving past debate on the dissociation of Tz.[9−12]

4. Conclusions

We report the first direct observation of two unique three-body dissociation mechanisms of Tz and the first observation

of experimental signatures of the dynamics proceeding through both conical and glancing JT intersections within one molecule. We found that the observed KER in the CE-induced three-body dissociation of Tz results from two different electronic states. The analysis of the product momentum partitioning obtained in coincidence experiments revealed both symmetric and asymmetric dissociation. The former was observed in the KER region between 2 and 4 eV, whereas the latter occurred between 1.5 and 5 eV. This energy dependence suggests that the symmetric dissociation proceeds through an excited electronic state of Tz populated in the resonance regime, while an off-resonant electronic state is responsible for the asymmetric breakup. Neglecting possible involvement of other electronic states, these observations can be explained within the reflection principle framework, assuming vibrational equilibration of the initially populated electronic state prior to a nonadiabatic transition to the ground state and fast dissociation on the ground-state PES. With the above provisions, the reflection principle attributes symmetric dissociation to an initial electronic state with symmetric equilibrium geometry and asymmetric dissociation to one with lower symmetry. Ab initio calculations and the analysis of the topology of the JT manifolds identified these states as the two highest valence states from the $\pi^* \leftarrow n$ manifold and the lowest 3s Rydberg state, respectively. The energy defect for $\pi^* \leftarrow n$ states is smaller than that of the Rydberg state; however, the coupling strength for the latter is two orders of magnitude larger, which explains the dominant presence of asymmetric breakup. These results are in agreement with the conclusions made by Ondrey et al., who suggested that Tz does not reach an equilibrium prior to dissociation and thus the partitioning of momentum to the HCN products depends heavily on the region of configuration space in which the ground-state surface was accessed (i.e., the entrance channel), while the final partitioning of internal energy in the products is determined by evolution on the dissociative surface.[7]

Acknowledgment. J.D.S., J.E.M., and REC are supported by the U.S. Air Force Office of Scientific Research under Grant No. FA9550-04-1-0035. V.M. and A.I.K. acknowledge support from the National Science Foundation (CHE-0616271). This work is conducted under the auspices of the iOpenShell Center for Computational Studies of Electronic Structure and Spectroscopy of Open-Shell and Electronically Excited Species supported by the National Science Foundation through the CRIF: CRF CHE-0625419 + 0624602 + 0625237 grant.

References and Notes

(1) Lee, Y.-P. State-resolved dynamics of photofragmentation. *Annu. Rev. Phys. Chem.* **2003**, *54*, 215.

(2) Maul, C.; Gericke, K.-H. Photo-induced three-body decay. *Int. Rev. Phys. Chem.* **1997**, *16*, 1.

(3) Maul, C.; Gericke, K.-H. Aspects of photo-induced molecular three-body decay. *J. Phys. Chem. A* **2000**, *104*, 2531.

(4) Ramsperger, H. C. The thermal decomposition of methyl isopropyl di-imide: A homogeneous unimolecular reaction. The thermal decomposition of hydrazolyc acid and methyl azide. *J. Am. Chem. Soc.* **1929**, *51*, 2134.

(5) Adams, N. G.; Poterya, V.; Babcock, L. M. Electron molecular ion recombination: Product excitation and fragmentation. *Mass. Spectrom. Rev.* **2006**, *25*, 798.

(6) Finlayson-Pitts, B. J.; Pitts, J. N. *Chemistry of the Upper and Lower Atmosphere: Theory, Experiments, and Applications*; Academic Press: New York, 1999.

(7) Ondrey, G. S.; Bersohn, R. Photodissociation dynamics of 1,3,5-triazine. *J. Chem. Phys.* **1984**, *81*, 4517.

(8) Gejo, T.; Harrison, J. A.; Huber, J. R. Three-body photodissociation of 1,3,5-triazine. *J. Chem. Phys.* **1996**, *100*, 13941.

(9) Dyakov, Y. A.; Mebel, A. M.; Lin, S. H.; Lee, Y. T.; Ni, C. K. Photodissociation of 1,3,5-triazine: An ab initio and RRKM study. *J. Phys. Chem. A* **2007**, *111*, 9591.

(10) Song, K. Y.; Collins, M. A. A classical trajectory study of sym-triazine photodissociation on an interpolated potential energy surface. *Chem. Phys. Lett.* **2001**, *335*, 481.

(11) Lee, J.; Dong, E. J.; Jin, D. S.; Song, K. Y.; Collins, M. A. Classical trajectory studies of the photodissociation reaction of sym-triazine. *Phys. Chem. Chem. Phys.* **2004**, *6*, 945.

(12) Pai, S. V.; Chabalowski, C. F.; Rice, B. M. Ab initio study of reactions of sym-triazine. *J. Phys. Chem.* **1996**, *100*, 5681.

(13) Osamura amd, Y.; Hashimoto, K. Theoretical-study of the photo-decomposition of s-triazine. *J. Am. Chem. Soc.* **1987**, *109*, 1370.

(14) Continetti, R. E. Coincidence spectroscopy. *Annu. Rev. Phys. Chem.* **2001**, *52*, 165.

(15) Laperle, C. M.; Mann, J. E.; Clements, T. G.; Continetti, R. E. Three-body dissociation dynamics of the low-lying Rydberg states of H_3 and D_3. *Phys. Rev. Lett.* **2004**, *93*, 153202.

(16) Galster, U.; Baumgartner, F.; Muller, U.; Helm, H.; Jungen, M. Experimental and quantum-chemical studies on the three-particle fragmentation of neutral triatomic hydrogen. *Phys. Rev. A* **2005**, *72*, 062506.

(17) Salop, A.; Lorents, D. C.; Peterson, J. R. Charge-transfer excitation produced in collisions of He^+ and N_2^+ with alkali atoms. *J. Chem. Phys.* **1971**, *54*, 1187.

(18) Sidis, V. Theory of dissociative charge-exchange in ion−molecule collisions. *J. Phys. Chem.* **1989**, *93*, 8128.

(19) Vanderzande, W. J.; Koot, W.; Peterson, J. R.; Los, J. Charge-exchange of O_2^+ with Cs - Spectroscopy and predissociation pathways for the π_g Rydberg states of O_2. *Chem. Phys. Lett.* **1987**, *140*, 175.

(20) Schinke, R. *Photodissociation Dynamics*; Cambridge Monographs on Atomic, Molecular, and Chemical Physics. Cambridge University Press: New York, 1993.

(21) Fridh, C.; Asbrink, L.; Jonsson, B. O.; Lindholm, E. Rydberg series in small molecules XIV: Photoelectron, UV, mass and electron impact spectra of s-triazine. *Int. J. Mass. Spectrom. Ion Phys.* **1972**, *8*, 85.

(22) P Debruijn, D.; Neuteboom, J.; Sidis, V.; Los, J. A detailed experimental-study of the dissociative charge-exchange of H_2^+ with Ar, Mg, Na and Cs targets at KeV energies. *Chem. Phys.* **1984**, *85*, 215.

(23) Kim, M. H.; Shen, L.; Tao, H.; Martinez, T. J.; Suits, A. G. Conformationally controlled chemistry: Excited-state dynamics dictate ground-state reaction. *Science* **2007**, *315*, 1561.

(24) Mozhayskiy, V. A.; Krylov, A. I. Analysis of equilibrium structures of electronically excited states of sym-triazine. *J. Phys. Chem.* **2008**, in preparation.

(25) Savee, J. D.; Mozhayskiy, V. A.; Mann, J. E.; Krylov, A. I.; Continetti, R. E. The role of the excited state topology in three-body dissociation of sym-triazine. *Science* **2008**, *321*, 826.

(26) Hanold, K. A.; Luong, A. K.; Clements, T. G.; Continetti, R. E. Photoelectron-multiple-photofragment coincidence spectrometer. *Rev. Sci. Instrum.* **1999**, *70*, 2268.

(27) Lampton, M.; Siegmund, O.; Raffanti, R. Delay-line anodes for microchannel-plate spectrometers. *Rev. Sci. Instrum.* **1987**, *58*, 2298.

(28) Continetti, R. E.; Cyr, D. R.; Osborn, D. L.; Leahy, D. J.; Neumark, D. M. Photodissociation dynamics of the N_3 radical. *J. Chem. Phys.* **1993**, *99*, 2616.

(29) Dalitz, R. H. On the analysis of tau-meson data and the nature of the tau-meson. *Philos. Mag.* **1953**, *44*, 1068.

(30) Savee, J. D., Mann, J. E., Continetti, R. E. 2008, in preparation.

(31) Sekino, H.; Bartlett, R. J. A linear response, coupled-cluster theory for excitation energy. *Int. J. Quantum Chem. Symp.* **1984**, *18*, 255.

(32) Koch, H.; Aa, H. J.; Jørgensen, P.; Helgaker, T. Excitation energies from the coupled clusters singles and doubles linear response functions (CCSDLR). Applications to Be, CH^+, CO, and H_2O. *J. Chem. Phys.* **1990**, *93*, 3345.

(33) Stanton, J. F.; Bartlett, R. J. The equation of motion coupled-cluster method. A systematic biorthogonal approach to molecular excitation energies,transition probabilities, and excited state properties. *J. Chem. Phys.* **1993**, *98*, 7029.

(34) Krylov, A. I. Equation-of-motion coupled-cluster methods for open-shell and electronically excited species: The hitchhiker's guide to Fock space. *Annu. Rev. Phys. Chem.* **2008**, *59*, 433.

(35) Sinha, D.; Mukhopadhyay, D.; Mukherjee, D. A note on the direct calculation of excitation-energies by quasi-degenerate MBPT and coupled-cluster theory. *Chem. Phys. Lett.* **1986**, *129*, 369.

(36) Stanton, J. F.; Gauss, J. Analytic energy derivatives for ionized states described by the equation-of-motion coupled cluster method. *J. Chem. Phys.* **1994**, *101*, 8938.

(37) Glendening, E. D.; Feller, D.; Thompson, M. A. An ab-initio investigation of the structure and alkali-metal cation selectivity of 18-crown-6. *J. Am. Chem. Soc.* **1994**, *116*, 10657.

(38) Mulliken, R. S. Molecular compounds and their spectra. II. *J. Am. Chem. Soc.* **1952**, *74*, 811.

(39) Cave, R. J.; Newton, M. D. Generalization of the Mulliken-Hush treatment of the calculation of electron transfer matrix elements. *Chem. Phys. Lett.* **1996**, *249*, 15.

(40) Demkov, Y. N. Charge transfer at small resonance defects. *Sov. Phys. JETP* **1964**, *18*, 138.

(41) Shao, Y.; Molnar, L. F.; Jung, Y.; Kussmann, J.; Ochsenfeld, C.; Brown, S.; Gilbert, A. T. B.; Slipchenko, L. V.; Levchenko, S. V.; O'Neil, D. P.; Distasio Jr, R. A.; Lochan, R. C.; Wang, T.; Beran, G. J. O.; Besley, N. A.; Herbert, J. M.; Lin, C. Y.; Van Voorhis, T.; Chien, S. H.; Sodt, A.; Steele, R. P.; Rassolov, V. A.; Maslen, P.; Korambath, P. P.; Adamson, R. D.; Austin, B.; Baker, J.; Bird, E. F. C.; Daschel, H.; Doerksen, R. J.; Drew, A.; Dunietz, B. D.; Dutoi, A. D.; Furlani, T. R.; Gwaltney, S. R.; Heyden, A.; Hirata, S.; Hsu, C.-P.; Kedziora, G. S.; Khalliulin, R. Z.; Klunziger, P.; Lee, A. M.; Liang, W. Z.; Lotan, I.; Nair, N.; Peters, B.; Proynov, E. I.; Pieniazek, P. A.; Rhee, Y. M.; Ritchie, J.; Rosta, E.; Sherrill, C. D.; Simmonett, A. C.; Subotnik, J. E.; Woodcock, H. L., III.; Zhang, W.; Bell, A. T.; Chakraborty, A. K.; Chipman, D. M.; Keil, F. J.; Warshel, A.; Herhe, W. J.; Schaefer, H. F., III.; Kong, J.; Krylov, A. I.; Gill, P. M. W.; Head-Gordon, M. Advances in methods and algorithms in a modern quantum chemistry program package. *Phys. Chem. Chem. Phys.* **2006**, *8*, 3172.

(42) Berson, J. A. Orbital-symmetry-forbidden reactions. *Acc. Chem. Res.* **1972**, *5*, 406.

(43) Borden, W. T.; Loncharich, R. J.; Houk, K. N. Synchronicity in multibond reactions. *Annu. Rev. Phys. Chem.* **1988**, *39*, 213.

(44) Dewar, M. J. S.; Jie, C. X. Mechanisms of pericyclic-reactions - the role of quantitative theory in the study of reaction-mechanisms. *Acc. Chem. Res.* **1992**, *25*, 537.

(45) Houk, K. H.; González, J.; Li, Y. Pericyclic reaction transition states: Passions and punctilios, 1995−1935. *Acc. Chem. Res.* **1995**, *28*, 81.

(46) Wilsey, S.; Houk, K. N.; Zewail, A. H. Ground- and excited-state reactions of norbornene and isomers: A CASSCF study and comparison with femtosecond experiments. *J. Am. Chem. Soc.* **1999**, *121*, 5772.

(47) Osamura, Y.; Schaefer, H. F.; Dupuis, M.; Lester, W. A. A unimolecular rection ABC → A + B + C involving three product molecules and a single transition state. Photodissociation of glyoxal: HCOHCO → H_2 + CO + CO. *J. Chem. Phys.* **1981**, *75*, 5828.

(48) Mozhayskiy, V. A.; Babikov, D.; Krylov, A. I. Conical and glancing Jahn−Teller intersections in the cyclic trinitrogen cation. *J. Chem. Phys.* **2006**, *124*, 224309.

(49) Dillon, J. J.; Yarkony, D. R. Seams near seams: The Jahn−Teller effect in the $^1E''$ state of N_3^+. *J. Chem. Phys.* **2007**, *126*, 124113.

(50) Bystrom, K. The stabilization energy of 1,3,5-triazine derived from measurements of the enthalpies of combustion and sublimation. *J. Chem. Thermodyn.* **1982**, *14*, 865.

(51) Choi, H.; Baeck, K. K.; Martinez, T. J. Ab initio molecular dynamics with equation-of-motion coupled-cluster theory: Electronic absorption spectrum of ethylene. *Chem. Phys. Lett.* **2003**, *375*, 299.

(52) Choi, H.; Baeck, K. K.; Martinez, T. J. Ab initio equation-of-motion coupled-cluster molecular dynamics with 'on-the-fly' diabatization: The doublet-like feature in the photoabsorption spectrum of ethylene. *Chem. Phys. Lett.* **2004**, *398*, 407.

(53) Bolovinos, A.; Tsekeris, P.; Philis, J.; Pantos, E.; Andritsopoulos, G. Absolute vacuum ultraviolet-absorption spectra of some gaseous azabenzenes. *J. Mol. Spectrosc.* **1984**, *103*, 240.

(54) K Innes, K.; G Ross, I.; Moomaw, W. R. Electronic states of azabenzenes and azanaphthalenes - A revised and extended critical-review. *J. Mol. Spectrosc.* **1988**, *132*, 492.

(55) Parusel, A. B. J.; Kohler, G.; Nooijen, M. A coupled-cluster analysis of the electronic excited states in aminobenzonitriles. *J. Phys. Chem. A* **1999**, *103*, 4056.

(56) Oliva, J. M.; Azenha, E. M. D. G.; Burrows, H. D.; Coimbra, R.; de Melo, J. S. S.; Canle, M. L.; Fernandez, M. I.; Santaballa, J. A. and L. Serrano-Andres On the low-lying excited states of sym-triazine-based herbicides. *ChemPhysChem* **2005**, *6*, 306.

(57) Kolaitis, L.; Lubman, D. M. Atmospheric-pressure ionization mass-spectrometry with laser-produced ions. *Anal. Chem.* **1986**, *58*, 1993.

(58) Kato, H.; Hirao, K.; Yamashita, K. Theoretical study on the Jahn-Teller distortion of pi- and n-cations of s-triazine. *J. Mol. Struct.: THEOCHEM* **1982**, *22*, 265.

(59) The averaging is performed as follows. The average of $\sin^2(x) = \int_{\mathfrak{V}} \sin^2(x)dx]\cdot\pi = (\pi/2)\cdot\pi = 1/2$. However, we have the average of $\sin^2(1/x)$, which is 1/2 at the region of oscillations (averaged over the period, period increases, or averaged over the oscillating region), and then it decreases to 0 when oscillations die down at large x. Thus, we employ averaging over the period, which yields an effective value of 0.5.

JP806369S